Elastic electron scattering by the CF_3 radical in the 1–1000 eV energy range

2017 J. Phys. B: At. Mol. Opt. Phys. 50 135201

(http://iopscience.iop.org/0953-4075/50/13/135201)

IOP Publishing Journal of Physics B: Atomic, Molecular and Optical Physics
J. Phys. B: At. Mol. Opt. Phys. **50** (2017) 135201 (11pp) https://doi.org/10.1088/1361-6455/aa739f

Elastic electron scattering by the CF_3 radical in the 1–1000 eV energy range

Sh Sh Demesh[1,2,3], V I Kelemen[1] and E Yu Remeta[1]

[1] Institute of Electron Physics, Ukrainian Academy of Sciences, Universitetska St. 21, 88017 Uzhhorod, Ukraine
[2] Institute for Nuclear Research, Hungarian Academy of Sciences, Bem tér 18/c, 4026 Debrecen, Hungary

E-mail: demes.sandor@atomki.mta.hu and remetov@inbox.ru

Received 30 November 2016, revised 4 April 2017
Accepted for publication 17 May 2017
Published 12 June 2017

Abstract

Elastic scattering of electrons by a CF_3 radical has been studied theoretically in a wide energy range of 1–1000 eV in the framework of an independent-atom model (IAM). The optical potential method is used for calculating the electron scattering amplitudes of the different atoms of the target molecule. The differential and integral cross sections are calculated for equilibrium internuclear distances of the ground state of the CF_3 radical in two approaches—IAM and additivity rule (IAM-AR) approximations. The calculated cross sections are compared with the experimental data for $e + CF_3$ and $e + CF_3H$ scattering and with other theoretical results. It is justified that the IAM performs slightly better for the differential cross sections, while the simpler IAM-AR approximation describes the integral cross sections better.

Keywords: electron scattering, cross section, independent-atom model, optical potential

(Some figures may appear in colour only in the online journal)

1. Introduction

Studying the characteristics of electron scattering by the CF_4 (fluoromethane) molecule and its fluorocarbon radicals is of high importance in plasma (gas-discharge, low-temperature and industrial plasmas), gaseous laser and semiconductor processing technologies, as well as in atmospheric sciences and ecology. The cross sections for electron scattering by fluoromethanes are very important for modelling the low-temperature plasma processes and characteristics. Such plasma processes are widely used in industry. The high number of experimental and theoretical works in the investigation of electron scattering by the fluorocarbon radicals implies a significant demand for such data. These chemical species are fragmented in the plasma into various neutral and ionized radicals [1] (see also [2, 3] and references therein).

The properties of the CF_nX_{4-n} compounds with hydrogen ($X = H$) or halogen atoms ($X = Cl$, Br, I), where $n = 0-4$, are also actively studied because of their usage. For example, CF_3H is an important gas for etching SiO_2, while chlorofluorocarbon molecules are used in different technological applications. Studying the peculiarities of electron scattering by CF_n and CF_nX_{4-n} molecules, we obtained important theoretical data about the cross sections of the corresponding processes. The information about the structural properties and scattering characteristics of these molecules could be very useful in order to use them for structurally similar molecules, where the carbon atom is substituted by an atom of Si (silicon) or Ge (germanium) (see review [1]).

The potential scattering of electrons by molecules is mainly determined by the positions of the atomic core charges and by the electron density distribution of the molecule. Such a scattering process can be described by the corresponding interaction potentials. The experimental cross sections for elastic electron scattering by the CF_3 radical have notably large values, up to 20 eV impact energies [2, 3], which distinguishes it from other fluorocarbon radicals. For theoretical estimations in [2, 3] the independent-atom model (IAM) was used with screened additivity rule corrections (IAM-SCAR), both with and without a ground-state dipole correction. The results of Schwinger multichannel (SMC) calculations were also presented in [2, 3] in the static-exchange (SE) approximation [4] along with R-matrix theoretical results [5].

[3] Author to whom any correspondence should be addressed.

It should also be noted that the semi-empirical energy-dependent geometric additivity rule (EGAR) approximation, which is similar to the IAM-SCAR theory, is demonstrated in [6, 7] with integral cross section calculations of electron scattering by different molecules. This model takes into consideration the shielding effects due to the geometrical structure of the molecule with collision-energy-dependent corrections. It seems that this approach works better with complex polyatomic target molecules at intermediate and high collision energies.

In references [2] and [3], the experimental differential cross sections (DCSs) for electron scattering by the CF_3 radical are significantly higher than the theoretical results in the energy range of 7–20 eV. At 7 eV the deviation is about a factor of 10. The difference between the experimental data and theory decreases with the increasing energy of the incident electron. The measured integral cross sections (ICSs) are also considerably higher than the theoretical values for energies up to 25 eV. The largest difference between the experimental and calculated ICSs was observed at 7 eV, where the measured values were about seven times higher than the theoretical ones.

The experimental work with carbon or fluorine atoms is rather difficult due to their high reactivity. Nevertheless, the different compounds, which contain these atoms, are chemically passive, so measuring the characteristics of electron scattering by them is feasible. The detailed theoretical study of electron scattering for these atoms, provided in [8, 9], allows us to estimate or calculate the scattering characteristics of those molecules, which contain C and F atoms.

We have theoretically investigated the elastic electron scattering by the CF_3 radical in its ground state in the framework of the IAM and IAM-AR approximations, using the scattering amplitudes of carbon and fluorine atoms, calculated by the optical potential (OP) method. The obtained cross sections for $e + CF_3$ scattering are compared with the corresponding experimental results, and also with the data for the CF_3H molecule. In the latter case, we suppose, the additional hydrogen atom with a single *s*-shell electron does not significantly change the spatial and electronic structure of the CF_3 radical, unlike the Cl, Br or I halogens. This assumption is also confirmed by experiments [10–12] and SMC theoretical results [13] for the CF_3H molecule. Therefore, in our opinion, the experimental data for $e + CF_3H$ scattering can serve as an additional argument for the explanation of the peculiarities of $e + CF_3$ scattering.

2. Methods

2.1. Scattering characteristics

In order to study the behaviour of elastic differential and integral elastic, momentum transfer and viscosity cross sections of electron scattering by the molecules in the IAM framework [14–16], we have used the OP method [17, 18] for the description of potential scattering of electrons by the corresponding atoms. In the case of electron scattering by an *N*-atomic molecule, the following scattering amplitudes are used in the IAM framework [19] (atomic units are used throughout this work, unless otherwise noted):

$$F(\theta, E) = \sum_{m=1}^{N} f_m(\theta, E) \cdot \exp(\mathrm{i}\vec{s} \cdot \vec{r}_m),$$
$$G(\theta, E) = \sum_{m=1}^{N} g_m(\theta, E) \cdot \exp(\mathrm{i}\vec{s} \cdot \vec{r}_m). \quad (1)$$

Here $\vec{s} = \vec{k}_i - \vec{k}_f = k(\vec{n}_i - \vec{n}_f)$ is the momentum transfer vector, $\vec{k}_i$ and $\vec{k}_f$ are the initial and final momenta of the incident electron; $\vec{r}_m$ is the radius vector of the *m*th atomic core of the molecule (with respect to the centre of mass of the molecule); θ—scattering angle; E—the incident electron's energy, $E = k^2/2$; f_m and g_m are the direct and spin–flip electron scattering amplitudes for the *m*th atom of the molecule. The $\exp(\mathrm{i}k\vec{n}_\mathrm{i} \cdot \vec{r}_m)$ factors in $F(\theta, E)$ and $G(\theta, E)$ amplitudes in (1) correspond to the phase shifts of waves, due to the change of the position of the scattering centres $\vec{r}_m$ with respect to the origin of reference frame [14].

The DCS for elastic electron scattering in the IAM framework is obtained by averaging over the vibrational and rotational degrees of freedom of the molecule (see [14, 15, 19]):

$$\frac{\mathrm{d}\sigma_\mathrm{el}^\mathrm{IAM}}{\mathrm{d}\Omega} = \langle |F|^2 + |G|^2 \rangle, \quad (2)$$

The DCS defined by (2) may be expressed with the atomic amplitudes

$$\frac{\mathrm{d}\sigma_\mathrm{el}^\mathrm{IAM}}{\mathrm{d}\Omega} = \sum_m [|f_m(\theta, k)|^2 + |g_m(\theta, k)|^2] + \sum_m \sum_{n \neq m} [f_m(\theta, k) f_n^*(\theta, k) + g_m(\theta, k) g_n^*(\theta, k)] \times \exp(-\ell_{mn}^2 s^2/2) \cdot \frac{\sin(sr_{nm})}{sr_{nm}}, \quad (3)$$

where r_{nm} is the internuclear distance between *n*th and *m*th atoms of the molecule, and the ℓ_{mn} is the amplitude of the corresponding vibrations, while $s(\theta, k) = 2k \sin(\theta/2)$. The first sum of (3) is the direct term, which corresponds to the sum of squares of the absolute values of the atomic scattering amplitudes, as in the IAM-AR approximation. The IAM-AR cross section could be also determined by the sum of atomic DCSs: $\mathrm{d}\sigma_\mathrm{el}^\mathrm{IAM-AR}/\mathrm{d}\Omega = \sum_{n=1}^{N} \mathrm{d}\sigma_{\mathrm{el},n}/\mathrm{d}\Omega$. The second sum of (3) is the indirect term $\mathrm{d}\sigma_\mathrm{el}^\mathrm{Ind}/\mathrm{d}\Omega$, which arises from the product of crossing amplitudes. It contains the product of the scattering amplitudes of identical or different atoms, which are located at certain distances from each other within the molecule. The spatial structure of the molecule has an effect on the total $\mathrm{d}\sigma_\mathrm{el}^\mathrm{IAM}/\mathrm{d}\Omega$ DCS even due to this term. The behaviour and the peculiarities of the $\mathrm{d}\sigma_\mathrm{el}^\mathrm{IAM}/\mathrm{d}\Omega$ and $\mathrm{d}\sigma_\mathrm{el}^\mathrm{IAM-AR}/\mathrm{d}\Omega$ DCSs are determined by the angular and energy dependence of the cross sections for the constituent carbon $\mathrm{d}\sigma_{\mathrm{el,\,C}}/\mathrm{d}\Omega$ and fluorine $\mathrm{d}\sigma_{\mathrm{el,\,F}}/\mathrm{d}\Omega$ atoms.

The integral cross sections of elastic scattering are connected with each other in the mentioned IAM and IAM-AR approximations. They can be calculated by direct integration of the corresponding DCSs over the scattering angles.

Therefore, from $d\sigma_{el}^{IAM}/d\Omega$ we obtain:

$$\sigma_{el}^{IAM}(E) = 2\pi\int_0^{\pi} d\theta \sin\theta \frac{d\sigma_{el}^{IAM}(\theta, E)}{d\theta} = \sigma_{el}^{IAM-AR}(E) + \sigma_{el}^{Ind}(E), \quad (4)$$

where

$$\sigma_{el}^{IAM-AR}(E) = 2\pi\int_0^{\pi} d\theta \sin\theta \frac{d\sigma_{el}^{IAM-AR}(\theta, E)}{d\theta}, \quad (5)$$

while the indirect term is

$$\sigma_{el}^{Ind}(E) = 2\pi\int_0^{\pi} d\theta \sin\theta \frac{d\sigma_{el}^{Ind}(\theta, E)}{d\theta}. \quad (6)$$

The momentum transfer $d\sigma_{mom}^{IAM}/d\Omega$, $d\sigma_{mom}^{IAM-AR}/d\Omega$ and viscosity $d\sigma_{vis}^{IAM}/d\Omega$, $d\sigma_{vis}^{IAM-AR}/d\Omega$ cross sections can be calculated analogously from the corresponding DCSs in the IAM as well as in the IAM-AR approximations, using weighting functions $(1-\cos\theta)$ and $\sin^2\theta$, respectively (see [20]).

The integral elastic cross section $\sigma_{el}^{IAM-AR}(E)$ can be calculated also according to the optical theorem [14–16, 21]. For the IAM, this theorem coincides with the IAM-AR approximation [15, 16, 22, 23]. Therefore, according to equation (3) and supposing that $\sin(sr_{nm})/sr_{nm}|_{\theta\to 0} \to 1$ and $\sin(sr_{nm})/sr_{nm}|_{r_{nm}\to 0} \to 1$, the following expression should be obtained:

$$\sigma_{el}^{IAM-AR}(E) = \frac{4\pi}{k}\sum_{n=1}^{N}\mathrm{Im}[f_n(\theta=0, k)] = \sum_{n=1}^{N}\sigma_{el,n}(E), \quad (7)$$

where the spin–flip amplitude does not affect the cross section (see below), because $g_n(\theta=0, k)=0$. The optical theorem (7) in the case of $e + CF_3$ elastic scattering gives the following formula for the integral cross section: $\sigma_{el}^{IAM-AR}(E) = \sigma_{el,C}(E) + 3\sigma_{el,F}(E)$.

The total intensity of the electron beam, which is scattered by an N-atomic molecule, can be measured experimentally. It is proportional to $d\sigma_{el}^{IAM}/d\Omega$, while in the case of forward scattering ($\theta \to 0$) it is proportional to N^2. At the same time, according to the optical theorem, the ICS is determined by scattering on N number of atoms of the molecule. Therefore, the more accurate calculation of ICSs should be, according to equations (5) and (7), IAM-AR approximation, while for the DCS calculation—according to (2) and (3)—IAM approximation. We have compared the obtained results in both approximations. Note that the IAM-AR approximation was also used for DCS and ICS calculations in works [2, 3].

The IAM approach is valid under the conditions [14]: $k(r_{nm})_{min} \gg 1$ and $(r_{nm})_{min} \gg (a)_{max}$. The first condition is fulfilled for fast incident electrons, while the second one is the single scattering criterion. Here $(r_{nm})_{min}$ is the minimal distance between the atomic centres, while $(a)_{max}$ is the maximal interaction radius between the incident particle and the different atoms. For example, at 14 eV electron energy and $(r_{nm})_{min} = 2a_0$, where a_0 is the Bohr radius, the weaker inequality $k(r_{nm})_{min} > 1$ is already satisfied.

Using a sufficiently good, strictly quantum-mechanical description of electron scattering by the potential field of the molecule's atoms, allows us to describe the scattering by the whole molecule, in general, in the IAM framework. We expect that such a description of the molecular electron scattering could be accurate even at intermediate energies, when the simple inequality $k(r_{nm})_{min} > 1$ is satisfied. It should be noted, for example, that the IAM-SCAR method [22, 23] was originally proposed in order to use the IAM for medium or even low collision energies (less than 10 eV).

The electron–atom scattering amplitudes can be derived from the real partial phase shifts $\delta_\ell^{\pm}(E) = \varepsilon_\ell^{\pm}(E)$ (for real interaction OP) [24] or from the complex ones $\delta_\ell^{\pm}(E) = \varepsilon_\ell^{\pm}(E) + i\xi_\ell^{\pm}(E)$ (for complex OP, with the account of absorption effects) [20, 24]. Having the phase shifts $\delta_\ell^{\pm}(E) = \varepsilon_\ell^{\pm}(E) + i\xi_\ell^{\pm}(E)$, one may find the direct scattering amplitude

$$f_m(\theta, k) = \frac{1}{2ik}\sum_{\ell=0}^{\infty}\left\{(\ell+1)\left[\frac{\exp(2i\varepsilon_\ell^{+})}{\exp(2\xi_\ell^{+})} - 1\right] + \ell\left[\frac{\exp(2i\varepsilon_\ell^{-})}{\exp(2\xi_\ell^{-})} - 1\right]\right\}P_\ell(\cos(\theta)), \quad (8)$$

while the spin–flip scattering amplitude is

$$g_m(\theta, k) = \frac{1}{2ik}\sum_{\ell=1}^{\infty}\left[\frac{\exp(2i\varepsilon_\ell^{-})}{\exp(2\xi_\ell^{-})} - \frac{\exp(2i\varepsilon_\ell^{+})}{\exp(2\xi_\ell^{+})}\right]P_\ell^1(\cos(\theta)), \quad (9)$$

where $P_\ell(\cos(\theta))$ are the Legendre polynomials and $P_\ell^1(\cos(\theta))$ are the first order associated Legendre functions.

2.2. Optical potential

In order to find the phase shifts of the electron scattering by the atoms, we have used complex OP with imaginary part $V_A(r, E)$ (RSEPA approximation) [20] (see also SEPA approximation in [24])

$$V_{opt}^{\pm}(r, E) = V^{\pm}(r, E) + iV_A(r, E). \quad (10)$$

The $V_A(r, E)$ potential describes the absorption effects of the scattering. The real part of the OP does not contain any empirical or fitted parameters (RSEP approximation):

$$V^{\pm}(r, E) = V_S(r) + V_E(r, E) + V_P(r) + V_R(r, E) + V_{SO}^{\pm}(r, E). \quad (11)$$

The '±' sign in the spin–orbit interaction potential is related to the total angular momentum of the incident electrons: $j = \ell \pm 1/2$. It should be noted that the scalar-relativistic potential $V_R(r, E)$ is not included in the real part of the OP (11) in the SEPA approximation. The OP components—V_S, V_E, V_P, V_R and $V_{SO}^{\pm}$—are the static, exchange, polarization, scalar-relativistic and spin–orbit interaction potentials, respectively. These components are determined by the total and spin electron densities of the molecule's atoms in general. The electron densities could be calculated by different theoretical approaches: Thomas–Fermi, Hartree–Fock, density functional theory, etc.

The well-known analytical expressions could also be used for these quantities with the corresponding parameters, which is very convenient for the calculations (see, for example, [25]). We use such electron densities for the atoms, which are calculated in the Hartree–Fock approximation using the corresponding approximated parameters [25]. It should be noted that the OP's potential components could also be determined by the molecular electron densities, similarly as was carried out in the most recent approaches (see [26–30] and references therein).

The static potential is determined by the Coulomb-type interaction with the atomic cores (with charge Z) and atomic electrons (with $\rho(\vec{r})$ electron density) of the target [20, 24]:

$$V_S(r) = -\frac{Z}{r} + \int d\vec{r}\,' \frac{\rho(\vec{r}\,')}{|\vec{r} - \vec{r}\,'|}. \tag{12}$$

The spin–orbit interaction potential $V_{SO}^{\pm}(r, E)$, which is connected to the static potential $V_S(r)$, is used in the following form [31]:

$$V_{SO}^{\pm}(r, E) = \zeta^{\pm}(j, \ell)\frac{\chi}{r}\frac{dV_S}{dr}, \quad \chi = \alpha^2/[2 + \alpha^2(E - V_S)]. \tag{13}$$

Here $\zeta^{+}(j, \ell) = \ell/2$ for $j = \ell + 1/2$, while $\zeta^{-}(j, \ell) = -(\ell + 1)/2$ for $j = \ell - 1/2$, α is the fine-structure constant. The scalar part of the relativistic potential $V_R(r, E)$ (also connected to $V_S(r)$) is described by the following expression (see [32]):

$$V_R(r, E) = -\frac{\alpha^2}{2}V_S^2 + \frac{\chi}{4}\frac{d^2V_S}{dr^2} + \frac{3\chi^2}{8}\left(\frac{dV_S}{dr}\right)^2. \tag{14}$$

The exchange interaction potential is described by the local, spin-unpolarised inhomogeneous electron gas approximation (see [17, 20, 24]):

$$V_E(r, E) = -\frac{k_F(r)}{\pi}\left(1 + \frac{1 - \kappa^2}{2\kappa}\ln\left|\frac{1 + \kappa}{1 - \kappa}\right|\right), \tag{15}$$

where $k_F(r) = [3\pi^2\rho(r)]^{1/3}$, $\kappa(r, E) = k_s(r, E)/k_F(r)$, $[k_s(r, E)]^2 = k^2 + V(r, k^2/2)$, $k^2 = 2E$. The following model expression is used for the $V(r, k^2/2)$ potential function: $V(r, k^2/2) = [k_F(r)]^2 + 2I/[1 + (kr)^2/2]$, where I is the ionization energy of the target atom. In this approximation the exchange potential could be non-relativistic $V_E^N(r, E)$ or relativistic $V_E^R(r, E)$ for heavier atoms [20].

The polarization potential is also used in the local, spin-unpolarised inhomogeneous electron gas approximation (see [17, 20]). The parameter-free expression for correlation–polarization interaction of the electrons is used for the short-range (SR) polarization potential, i.e. in the inner region of the atom, where $V_P = V_P^{SR}$

$$V_P^{SR}(r) = \varepsilon_c(r_s) - \frac{r_s}{3}\frac{d\varepsilon_c}{dr_s}. \tag{16}$$

Here $\varepsilon_c[\rho(r)] = \varepsilon_c[r_s(r)]$ is the correlation energy density, $r_s(r) = \{3/[4\pi \cdot \rho(r)]\}^{1/3}$. At asymptotic, long-range (LR) distances the polarization potential has the following simple form: $V_P^{LR}(r) = -\alpha_d(0)/2r^4$. The $V_P^{SR}(r)$ and $V_P^{LR}(r)$ potentials cross each other at a certain r_c point.

The absorption effects give their contribution in the scattering characteristics at $E > \Delta_a$ collision energies, where Δ_a is the energy of the first inelastic threshold of the atom. In the case of carbon and fluorine atoms, such effects could be taken into consideration beginning from $\Delta_C = 7.50$ eV and $\Delta_F = 12.6968$ eV energies [33], respectively. It is equal to the mean energy of the $^3P^o$ term with a $2p3s$ electron configuration for the carbon atom, which is obtained by dipole-excitation from its $2p^2\,{}^3P_0$ ground-state (the ionization energy of the carbon is 11.260 eV) [33]. In the case of the fluorine atom, this is the energy of the $^4P_{5/2}$ term with a $2p^4 3s$ configuration, which can be obtained by excitation from its $2p^5\,{}^2P^o_{5/2}$ ground-state (the ionization energy in this case is 17.423 eV) [33].

The modified version two of the non-empirical Staszewska-type potential [34] is used for the $V_A(r, E)$ absorption potential. All versions of this absorption potential have the following general form in the quasi-free electron scattering model:

$$Vaf(r, E) = -\nu_{loc}(r, E) \cdot \rho(r) \cdot \overline{\sigma}_b(r, E)/2. \tag{17}$$

The modification of this potential lies in the following two aspects. First, the polarization potential, V_P, is taken into account in the expression for the incident electron's local velocity, so $\nu_{loc} = [2(E - V_{SEP})]^{1/2}$, where $V_{SEP} = V_S + V_E + V_P$. Second, the V_P potential is also included in the expressions for $\alpha(r, E)$ and $\beta(r, E)$ functions, which are used to determine the average cross section of binary collisions $\overline{\sigma}_b(r, E)$. Therefore, with the mentioned modification of $Vaf2m(r, E)$ absorption potential, these functions have the following forms: $\alpha = k_F^2 + \Delta - 2V_{SEP}$ and $\beta = \alpha$ (compare it with expression (21a) of [34]).

We have used the following energy-absorption model for the CF_3 radical. As the collision energy increases, starting from Δ_C, the absorption takes place due to the carbon atom. As the collision energy further increases, starting from $\Delta_C + \Delta_F$, one of the fluorine atoms is connected in the absorption scheme additionally. Above $\Delta_C + 2\Delta_F$ energies, two of the three fluorine atoms absorbs energy, while all of the atoms can absorb energy from $\Delta_C + 3\Delta_F$ and above. Accounting the absorption effects leads to a certain decreasing of the values of DCSs of elastic scattering, as well as of integral elastic, momentum transfer and viscosity cross sections.

It should also be noted that the absorption effects are taken into consideration more strictly in spherical [28, 29] and single-center [30] approximations, where they can be obtained by studying the excitation of electronic, vibrational and rotational spectra of the whole molecule, in general.

2.3. Scattering phase shifts calculation

The partial phase shifts for the incident electron's initial angular momenta values $\ell < \ell_{min}$ could be obtained by the variable-phase method by solving the coupled first-order nonlinear differential equations for real or complex phase functions (see [20, 24] and references therein) with the corresponding OP (10) or (11). For example, in the

case of complex OP (10), the absolute phase shift values $\delta_\ell^\pm(E) = \varepsilon_\ell^\pm(E) + i\xi_\ell^\pm(E)$ could be determined from the large distance limit of the phase functions $\varepsilon_\ell^\pm(r, E)$ and $\eta_\ell^\pm(r, E) = \exp[-2\xi_\ell^\pm(r, E)]$

$$\varepsilon_\ell^\pm(E) = \lim_{r\to\infty}\varepsilon_\ell^\pm(r, E),$$
$$\xi_\ell^\pm(E) = -\frac{1}{2}\ln[\lim_{r\to\infty}\eta_\ell^\pm(r, E)]. \quad (18)$$

The asymptotic values of the phase shifts for $\ell_{max} > \ell > \ell_{min}$ could be obtained by the following expression [21]:

$$\mathrm{tg}\delta_\ell^{as} = \pi\alpha_d(0)k^2/[(2\ell+3)(2\ell+1)(2\ell-1)], \quad (19)$$

where $\alpha_d(0)$ is the dipole static polarizability of the corresponding atom. We have used the 11.260 a_0^3 value for carbon and 3.76 a_0^3 for the fluorine atom [35].

2.4. Structural calculations of the CF_3 radical

All structural characteristics of the ground state of the CF_3 radical are calculated using the theoretical methods of the GAUSSIAN computer code [36]. In order to obtain the initial electron density matrix, self-consistent iterative calculations are performed by the unrestricted Hartree–Fock method. Further calculations are provided in order to adequately describe the correlation interaction of electrons, using the coupled cluster method with single and double excitation and triple corrections (CCSD(T) method). The augmented, correlation-consistent, polarized valence double-zeta (aug-cc-pvdz) Gaussian basis set is used for all calculations.

The equilibrium structural parameters for the ground state of the CF_3 radical are obtained by geometry optimization, using the quadratic approximation algorithm at the CCSD(T) level of theory. The calculated equilibrium interatomic distances are as follows (in a_0): $r_{12} = r_{13} = r_{14} = 2.5256$, $r_{23} = r_{24} = r_{34} = 4.1674$. Here the carbon atom is labelled by number 1, while the fluorine atoms—by numbers 2, 3 and 4. In order to obtain information about the excited electronic states of the CF_3 radical, further *ab initio* calculations were carried out. The lowest excited states of the radical were also calculated by the GAUSSIAN package, using the configuration interaction method with single and double excitations (CISD). According to these calculations, the electronically excited energy levels of the CF_3 radical are sufficiently high, the lowest of them is located at 7.86 eV.

3. Results and discussion

3.1. Integral cross sections for e + CF_3 scattering

The calculated integral elastic and momentum transfer cross sections of $e + CF_3$ scattering are shown in figures 1–2. Table 1 also shows, along with the above mentioned, the viscosity cross sections from 1 up to 1000 eV collision energies. The ℓ_{mn} amplitudes of vibrations from (3) are not taken into consideration, i.e. we suppose $\ell_{mn} = 0$ in the mentioned equation. A detailed description of the calculation technique for mean vibrational amplitude values can be found in [37]. The ICSs are also compared with the available experimental results for $e + CF_3$ [2, 3] and $e + CF_3H$ [1, 10, 11] scattering processes. It should be noted that the ICSs in [2, 3] were measured with quite large errors—80% at 50 eV and 60% at all other collision energies, while the errors in [10, 11] are considerably smaller, less than 30% (see figure 1). The integral elastic cross sections of electron

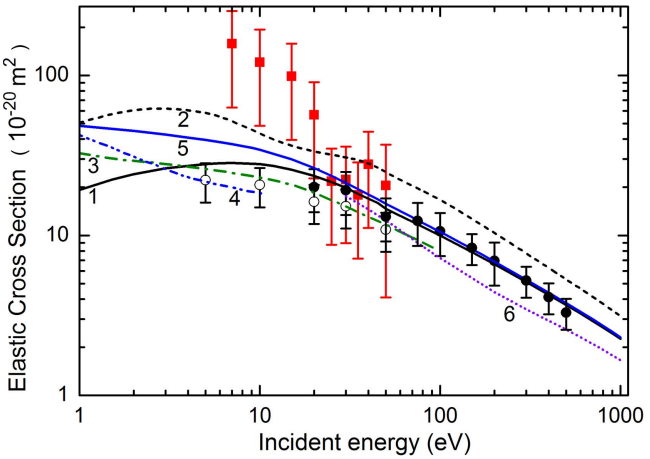

Figure 1. Energy dependence of the integral elastic cross sections of $e + CF_3$ scattering. Theory: $e + CF_3$—RSEPA IAM-AR approximation, present results (1, black solid), RSEPA IAM approximation, present results (2, black short dashed), IAM-SCAR calculations with a ground-state dipole correction [2, 3] (3, olive dash-dot), R-matrix calculations with a Born correction [5] (4, blue dash-dot-dot); $e + CF_3H$—RSEP IAM-AR approximation, present results (5, blue solid), SCOP [38] (6, violet short-dot). Experiment: $e + CF_3$—[2, 3] (red filled squares); $e + CF_3H$—[10] (black filled circles), [11] (black open circles).

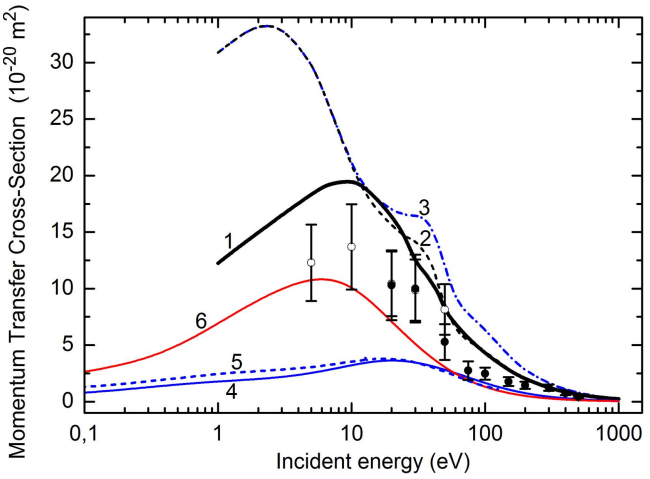

Figure 2. Energy dependence of the integral momentum transfer cross sections of $e + CF_3$ scattering. Theory: $e + CF_3$—RSEPA IAM-AR approximation, present results (1, black solid), RSEPA IAM approximation, present results (2, black short dashed), RSEP IAM approximation, present results (3, blue short dash-dotted); $e + F$—RSEP, present results (4, blue solid), BSR [9] (5, blue short dashed); $e + C$—RSEP, present results (6, red solid). Experiment: $e + CF_3H$—[10] (black filled circles), [11] (black open circles).

Table 1. Integral elastic $\sigma_{el}^{IAM-AR}(E)$, momentum-transfer $\sigma_{mom}^{IAM-AR}(E)$ and viscosity $\sigma_{vis}^{IAM-AR}(E)$ cross sections of electron scattering by the CF_3 radical (in units of 10^{-20} m^2). The cross sections were obtained in the RSEPA (10) IAM-AR approximation (7), where the *Vaf*2 (17) absorption potential is used.

E (eV)	σ_{el}^{IAM-AR}	σ_{mom}^{IAM-AR}	σ_{vis}^{IAM-AR}
1	19.2539	12.2521	12.4915
1.5	22.2495	13.8570	14.3711
2	24.1164	14.9628	15.5504
3	26.2564	16.5000	16.8544
5	27.9791	18.3591	17.5669
6	28.2822	18.9227	17.4732
7	28.3857	19.3086	17.2260
10	27.9122	19.5698	15.9552
12	27.1503	19.1461	14.8796
15	25.757	18.1316	13.2802
20	23.5469	16.4412	11.0852
25	21.5244	14.6956	9.23711
30	19.8964	12.3312	7.89479
35	18.1925	11.5465	6.53103
40	16.9943	10.4851	5.70344
45	15.9801	9.59563	5.06092
50	14.6886	8.07314	4.18942
60	13.2793	6.87731	3.47326
75	11.7377	5.62205	2.82821
100	9.9856	4.26854	2.26454
150	7.86798	2.77301	1.73909
200	6.59521	1.98982	1.44265
300	5.11277	1.21426	1.06524
400	4.25104	0.84173	0.82569
500	3.67118	0.62703	0.66169
600	3.24641	0.48944	0.54383
700	2.91812	0.39481	0.456
800	2.65477	0.32646	0.3886
900	2.4378	0.27518	0.33564
1000	2.2553	0.23559	0.29319

scattering by the carbon and fluorine atoms are shown in figure 3, along with the results of *B*-spline *R*-matrix (BSR) theory [8, 9].

As we have mentioned already, more correct values of the ICSs can be obtained using the IAM-AR approximation, when they are equal to the sum of the ICSs of atomic scattering. Likewise, as shown in figure 3, the scattering by the carbon atom plays the main role in these integral cross sections. The obtained ICSs in the IAM-AR approximation coincide with the experiments [2, 3] at 25, 30 and 35 eV collision energies, while at 40 and 50 eV they are slightly lower but still close to the measured ones. Our ICSs at energies from 1 to 10 eV go below the IAM-SCAR (with a ground-state dipole correction) theoretical results (see [2, 3]), while in the 40–50 eV energy region our values are higher. In general, the effect of this ground-state dipole correction quickly decreases (by an order of magnitude), when the scattering angle increases, so it has considerable effect to the ICSs at a relatively narrow forward scattering angle interval:

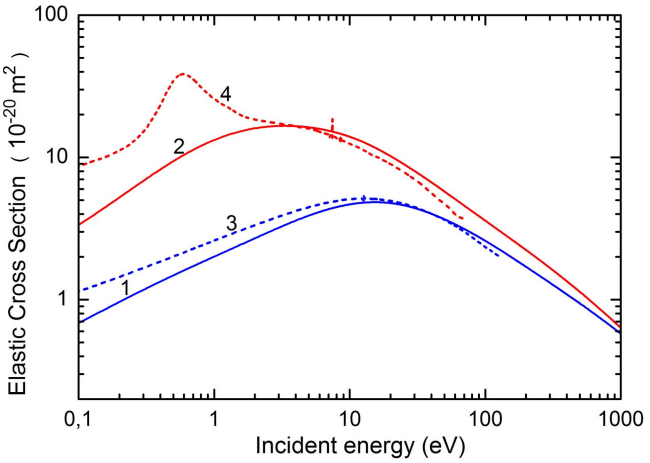

Figure 3. Energy dependence of the integral elastic cross sections of $e + C$ and $e + F$ scattering. Theory: $e + F$—RSEP, present results (1, blue solid), BSR [9] (3, blue short dashed); $e + C$—RSEP, present results (2, red solid), BSR [8] (4, red short dashed).

0°–20° at 7 eV and 0°–3° at 40 eV energy (see [2, 3]). While the collision energy decreases from 1 to 0.1 eV the cross sections from the R-matrix calculations with a Born correction [5] increase. In the 2–10 eV energy range the cross sections of [5] are lower than our and the IAM-SCAR cross sections. Our IAM calculations give overestimated results for the ICSs, due to the interference effect of the electron waves in the scattering process by the atoms of the molecule.

The experimental ICSs for the $e + CF_3H$ scattering at energies below 20 eV, as one can see in figure 1, are not similar to the $e + CF_3$ cross sections, i.e. does not take such high values. As the static dipole polarizabilities of the CF_3 radical (values from 5.81 to 19.52 a_0^3 are provided in [39]) and CF_3H molecule (23.754 a_0^3 [39]; 17.552 a_0^3 [13] and 23.889 a_0^3 (experiment [13])) are quite large, then the asymptotic behaviour of their polarization interaction potential should be very similar. In our opinion, the different behaviour of the ICSs of electron scattering by these molecules at low energies could be related mainly with their intrinsic electron density distribution. It should be noted that the spherical complex optical potential (SCOP) method was used to calculate the $e + CF_3H$ scattering cross sections in [38].

The electron density distribution isosurfaces for the CF_3 radical and CF_3H molecule are compared in figures 4(a)–(b), respectively. In order to analyse and compare the electron densities of the mentioned molecules, further *ab initio* calculations were performed by the GAMESS(US) quantum chemistry package [40]. New geometry optimization was carried out for both molecules on the DFT/B3LYP level of theory, using the aug-cc-pvdz basis set as well. The isosurfaces are constructed then by the wxMacMolPlt graphical visualizer program [41]. The electron density distribution for both molecules was plotted in the surface with 0.2 value. In other words, the surfaces in figure 4 visualize such molecular

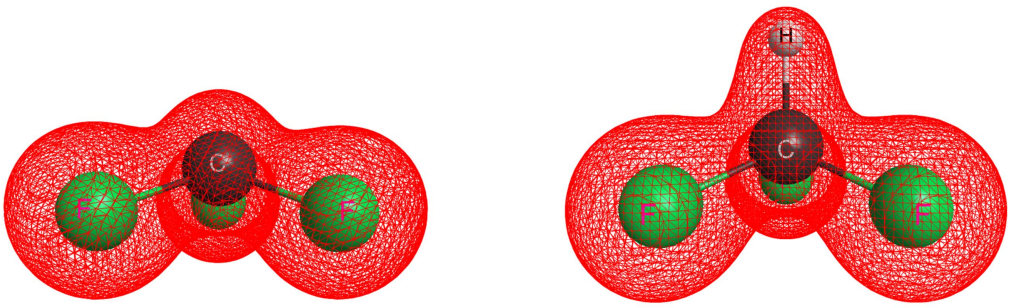

(a) (b)

Figure 4. The electron density distribution isosurfaces for CF_3 (a) radical and CF_3H (b) molecule.

space, where the normalized electron density for the given molecules equals to 0.2. As one can see in the calculated isosurfaces, the single hydrogen atom of the CF_3H molecule comparably weakly distorts the general electron picture of this molecule. Therefore, even such a distortion can play an important role in low-energy collisions (below 20 eV), when the incident electron has enough time to interact with the 'loose' electron cloud, which characterizes the molecular field between the carbon and hydrogen atoms. A faster incident particle could go across this region, not interacting with its electrons. It also should be noted that the bond order for the C–H bond in the CF_3H molecule, calculated by a CCSD(T) population analysis, is higher (0.966) than it is for the C–F bonds (0.780) of the same molecule. This indicates that the electrons between the C and H atoms are more localized and bound. The calculated value of the C-F bond order in the CF_3 radical is 0.873, which proves that the presence of a single hydrogen atom leads to a slight perturbation of the whole electron cloud of the molecule.

The equilibrium interatomic distances for the CF_3H molecule, according to the CCSD(T) calculations, are as follows (in a_0): $r_{CF} = 2.5579$, $r_{CH} = 2.0780$, $r_{HF} = 3.8219$ and $r_{FF} = 4.1457$. The calculated interatomic distances for the CF_3 radical (which were mentioned earlier): $r_{CF} = 2.5256$, $r_{FF} = 4.1674$.

The energy dependencies of the experimental integral elastic cross sections for $e + CF_3H$ scattering [10, 11] (figure 1) as well as the momentum transfer ICSs [10, 11] (figure 2) are very similar to our calculated ICSs for $e + CF_3$ scattering in the IAM-AR approximation, in the whole energy range. The theoretical cross sections, obtained by the IAM-SCAR calculations, are shown in [2] both with and without a ground-state dipole correction. Taking into account of this correction slightly increases the ICSs, when the collision energy decreases from 10 eV to 1 eV. The closest results to the experiments were achieved by the IAM-SCAR calculations at 25–35 eV energies in [2], where the ground-state dipole correction is not important.

The results of *R*-matrix calculations [5] are also provided in [2], both with and without a Born correction. The effect of this correction also increases, as the collision energy decreases from 10 eV to 0.1 eV. The ICSs, obtained by the *R*-matrix calculations, rapidly increase at energies below 1 eV, which states the necessity of description of electron scattering by the molecule as a whole. It should also be noted, that the *R*-matrix results with a Born correction are lower than the IAM-SCAR values at 7 and 10 eV, where this correction is not important (see figure 1).

We suppose the integral cross sections' behaviour and amplitudes should be very different depending on the electron scattering by excited or ground-state molecules. In the first step, the target molecule could be vibrationally excited from ~0.1 eV. Beginning from the energies of the molecule's first excited electronic states, which is usually on the level of a few eV, electronic excitation processes can take place as well. Some examples of electron scattering by excited atoms and molecules are given in [42]. Therefore, for the completeness of the theoretical description of the scattering process, it is necessary to take into consideration the scattering on the vibrationally excited CF_3 radical as well. On the other hand, while dealing with scattering by the CF_3 radical in its ground-state, the imaginary part of the optical potential, which is responsible for the inelastic processes of scattering (different types of excitation, ionization), should be considered from very low (around zero eV) incident electron energies.

3.2. Differential cross sections for e + CF_3 scattering

The calculated DCSs for $e + CF_3$ elastic scattering by the RSEP and the RSEPA theory of the IAM and the IAM-AR approximations are shown in figure 5 at 7, 10, 15, 20, 25, 30, 35, 40, 45, 50, 75 and 100 eV collision energies. We have compared their angular behaviour with the experimental data for $e + CF_3$ [2, 3] and $e + CF_3H$ [10, 11, 13] scattering (see also [1, 12]). It should be noted here that the DCSs in [11] were measured nearly in the whole angular range—5°–180°. While the DCSs in [2, 3] are characterized with especially large errors (from 35% up to 100%, depending on the scattering angles and collision energies), at the same time they are considerably smaller for all angles and energies in [11–13]—15%–30%, 15%–20% and 8%–15%, respectively.

The more correct results of the DCSs, unlike the ICSs, can be obtained by the IAM approximation, taking into account the interference of scattering waves by the atoms. The IAM-AR approximation gives the sum of the atomic

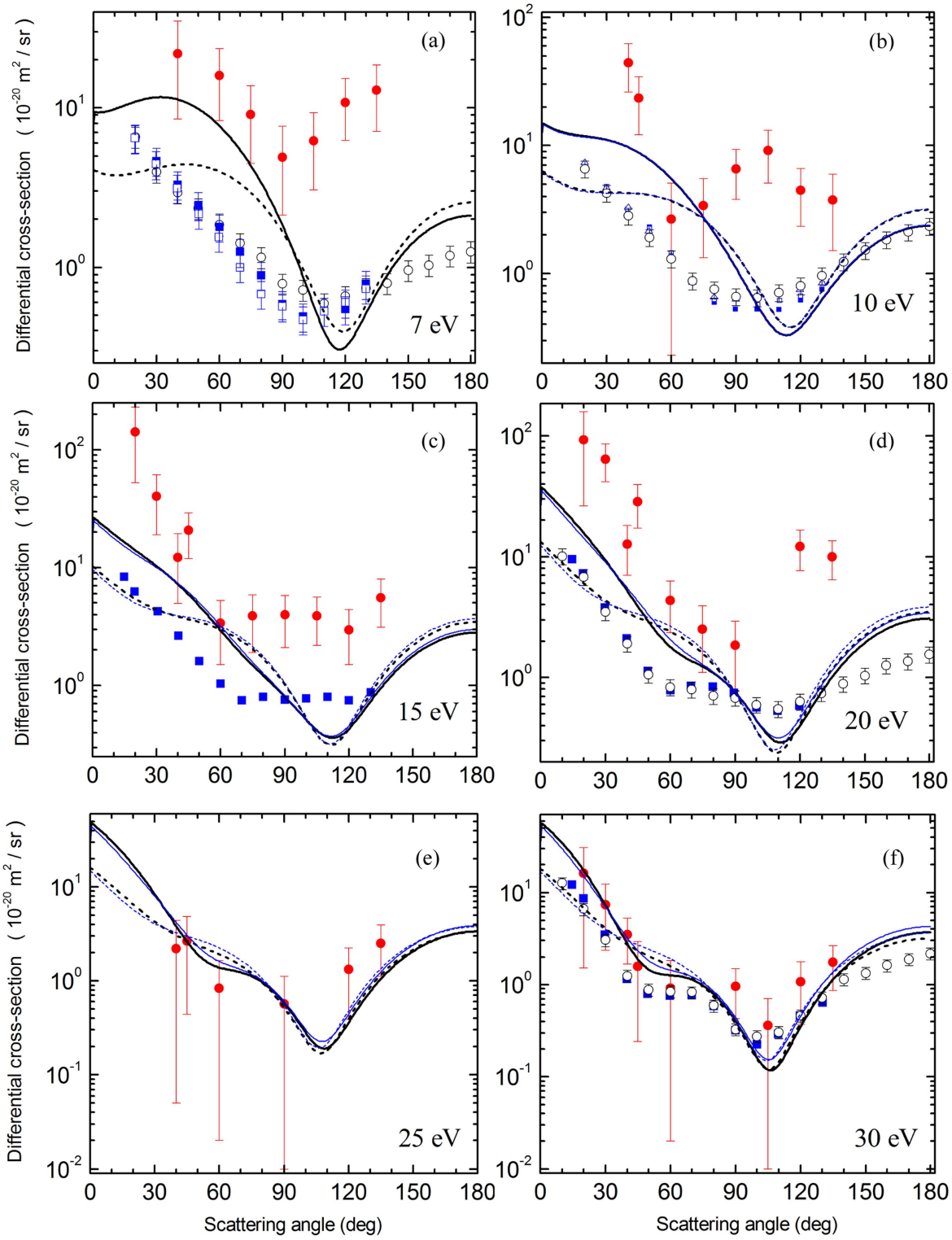

Figure 5. Angular dependences of DCSs for $e + CF_3$ scattering at 7 (a), 10 (b), 15 (c), 20 (d), 25 (e), 30 (f), 35 (g), 40 (h), 45 (i), 50 (j), 75 (k) and 100 (l) eV energies.Theory: RSEPA, present results—IAM approximation (thick black solid), IAM-AR approximation (thick black short dashed); RSEP, present results—IAM approximation (thin blue solid), IAM-AR approximation (thin blue short dashed). Experiment: $e + CF_3$ [2, 3] (red filled circles); $e + CF_3H$ [13] (blue open squares)—(a) 6.5 eV, (b) 9 eV; (blue filled squares)—(a) 7 eV, (b) 8 eV, (c) 15 eV, (d) 20 eV, (f) 30 eV; (blue open triangles)—(b) 10 eV; $e + CF_3H$ [10] (black triangle)—(j) 50 eV, (k) 75 eV, (l) 100 eV; $e + CF_3H$ [11] (black open circles)—(a) 5 eV, (b) 10 eV, (d) 20 eV, (f) 30 eV, (j) 50 eV.

scattering DCSs, so it can lead to underestimated DCS values. Comparing these two approaches we could draw the corresponding conclusions about the role of interference effects in the electron scattering process by the atoms of the molecule, as well as about the contribution of individual atomic scattering cross sections.

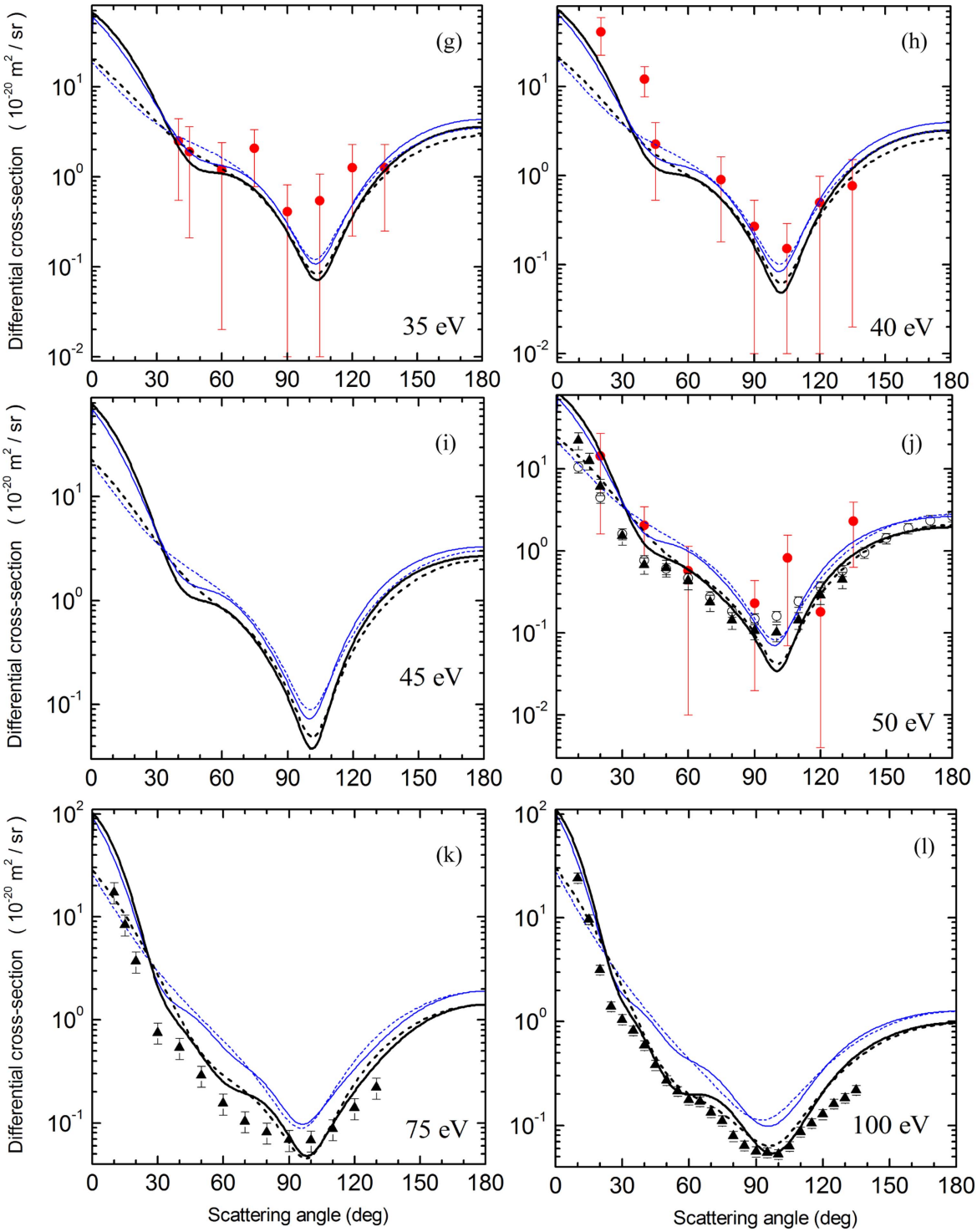

Figure 5. (Continued.)

The quantitative contribution, arising from the interference effects is appreciable at scattering angles up to 90° in general. For example, such contribution at 7 eV collision energy is considerable in a wide angular range—from 0 to 90°. This angular range is restricted to about [0°, ~25°] at 100 eV. Taking into account the interference effects of the IAM approximation at sufficiently high, 75 and 100 eV, energies, one can obtain an oscillating structure in the DCSs. Our calculated DCSs in the IAM and IAM-AR approximations are very similar in their forms at all investigated energies in general.

The absorption effects do not distort the angular behaviour of the DCSs, but somewhat decrease their amplitudes, except at lower energies (up to 30 eV), where the RSEPA DCSs are slightly higher the RSEP DCSs.

In accordance with our preliminary expectations, our calculated DCSs by the IAM approximation are somewhat

higher in amplitude and they are closer to the experimental data of [2, 3]. They can reproduce the angular behaviour of the experimental DCSs from 20 eV and above. Therefore, it could be stated that our DCSs are close to the experimental ones even from these energies and above. At the same time it should be noted that the angular dependencies of the experimental DCSs are smooth at all collision energies in general, however the measured DCS suddenly decreases at 10 eV in the 40°–60° angular range. It should be noted that the RSEPA DCSs in the IAM approximation are closer to the experimental data, even at a comparably large 50 eV energy, as we can see in figure 5(j). Obviously, taking into consideration the absorption effects brings these DCS values closer to the experiment. These cross sections also highly overestimate the DCSs of the IAM-AR approximation at low scattering angles, below 30°.

Comparing the experimental DCSs for the $e + CF_3H$ scattering with the $e + CF_3$ data shows a similarity between their angular behaviour in general, except at 10 eV (see figures 5(a)–(d), (f)). The DCSs for these processes and our DCSs in the IAM approximation adequately coincide above energies of 30 eV .

As one can see, in [2, 3] the calculated DCSs on the basis of a molecular description of scattering—*R*-matrix [5], SMC [4] and SMC static-exchange (SMC-SE, see [3]) theories—are qualitatively more similar to the experimental angular behaviour at low—7, 10, 15 and 20 eV—energies. These results state the necessity of taking into account the molecular characteristics, as a whole, for such kind of calculations. Nevertheless, the values of the mentioned theoretical DCSs are considerably smaller as compared with the experimental ones. The IAM-SCAR DCSs of [2, 3] are also similar to our results, obtained by the IAM-AR approximation.

4. Conclusions

The IAM framework along with the parameter-free real and complex optical potential methods (for electron–atom interactions) are used for the description of potential scattering of electrons by the CF_3 radical in its ground state. There is a good agreement between our calculated integral cross sections above 25 eV and DCSs above 20 eV as compared with the experimental data. A convincing description of scattering characteristics—integral and DCSs—was obtained by calculations according to the optical theorem. In our opinion, the DCSs' angular behaviour is described rather well in the IAM from average angles at low energies. At higher energies the description is rather good from lower angles as well, while taking into consideration the interference effects of the scattering waves from the atoms of molecule. In the IAM, the peculiarities of all cross sections for electron–molecule scattering unambiguously depend on the peculiarities of the corresponding electron–atom scattering cross sections.

Taking into account the absorption effects leads to a slight decreasing of integral cross section values, but it rather poorly affects the angular behaviour and the amplitudes of the DCSs.

Comparing the calculated cross sections of low-energy electron scattering by the CF_3 radical with the available experimental data for CF_3 radical and CF_3H molecule calls for calculations with purely molecular characteristics—electron densities and with the corresponding interaction potentials—as highly necessary for the correct description of the mentioned electron–molecule scattering processes. This could lead to a more successful application of different theoretical methods at low collision energies. Presumably, just such a description of electron scattering can lead to an overall qualitative and quantitative explanation of the electron scattering process by the CF_3 radical, where along with the structural characteristics of the target molecule, the dynamic response of its electrons to the incident electron's field is concerned. It is also worth taking into account the absorption effects from very low energies during the calculations, especially the vibrationally excited states of the molecules.

Our theoretical results for the $e + CF_3$ scattering cross sections, along with other calculations with different methods, describe the CF_3 radical only in its ground state. The highest deviation between all theoretical cross sections and the experimentally measured data was observed at low collision energies, below 15 eV, which, in our opinion, is apparently related to the electron scattering by the vibrationally excited radical.

Acknowledgments

SD gratefully acknowledges the International Visegrad Fund (Grants No. 51501167 and 51600934) for the support of this scientific research. The HPC supercomputer support from the Hungarian NIIF Institution is also acknowledged. The authors are grateful to Z Juhász and L Gulyás for the fruitful discussions.

References

[1] Yoon J-S, Song M-Y, Kato H, Hoshino M, Tanaka H, Brunger M J, Buckman S J and Cho H 2010 *J. Phys. Chem. Ref. Data* **39** 033106
[2] Brunton J R, Hargreaves L R, Buckman S J, García G, Blanco F, Zatsarinny O, Bartschat K and Brunger M J 2013 *Chem. Phys. Lett.* **568–569** 55–8
[3] Brunton J R *et al* 2013 *J. Phys. B: At. Mol. Opt. Phys.* **46** 245203–11
[4] Diniz R B, Lima M A P and da Paixao F J 1999 *J. Phys. B: At. Mol. Opt. Phys.* **32** L539
[5] Rozum I and Tennyson J 2004 *J. Phys. B: At. Mol. Opt. Phys.* **37** 957
[6] Jiang Y, Sun J and Wan L 1997 *Phys. Lett.* A **237** 53–7
[7] Jiang Y, Sun J and Wan L 1997 *J. Phys. B: At. Mol. Opt. Phys.* **30** 5025–32
[8] Zatsarinny O, Bartschat K, Bandurina L and Gedeon V 2005 *Phys. Rev.* A **71** 042702
[9] Gedeon V, Gedeon S, Lazur V, Nagy E, Zatsarinny O and Bartschat K 2014 *Phys. Rev.* A **89** 052713

[10] Iga I, Rawat P, Sanches I P, Lee M-T and Homem M G P 2005 *J. Phys. B: At. Mol. Opt. Phys.* **38** 2319
[11] Cho H, Song M Y, Yoon J S, Hoshino M and Tanaka H 2010 *J. Phys. B: At. Mol. Opt. Phys.* **43** 135205–13
[12] Tanaka H, Masai T, Kimura M, Nishimura T and Itikawa Y 1997 *Phys. Rev.* A **56** R3338–41
[13] Varella M T D N, Winstead C, McKoy V, Kitajima M and Tanaka H 2002 *Phys. Rev.* A **65** 022702–19
[14] Mott N F and Massey H S W 1965 *The Theory of Atomic Collisions* (Oxford: University Press) p 858
[15] Raj D 1991 *Phys. Lett.* A **160** 571
[16] Mozejko P, Zywicka-Mozejko B and Szmytkowski C 2002 *Nucl. Instr. Meth.* B **196** 245
[17] Demesh S, Remeta E and Kelemen V 2014 Elastic electron scattering on molecule in optical potential approach *Contrib. Pap. 6th Conf. Elem. Proc. At. Sys. (CEPAS)* ed Š Matejčík *et al* (Bratislava: Comenius University) pp 65–6
[18] Demesh S S, Kelemen V I and Remeta E Y 2015 *J. Phys.: Conf. Ser.* **635** 072020
[19] Yates A C 1968 *Phys. Rev.* **176** 173
[20] Kelemen V I and Remeta E Y 2012 *J. Phys. B: At. Mol. Phys.* **45** 185202
[21] Burke P G 1977 *Potential Scattering in Atomic Physics* (New York: Plenum) p 138
[22] Blanco F and García G 2003 *Phys. Lett.* **A317** 458
[23] Blanco F and García G 2004 *Phys. Lett.* **A330** 230
[24] Kelemen V, Remeta E and Sabad E 1995 *J. Phys. B: At. Mol. Opt. Phys.* **28** 1527
[25] Strand T G and Bonham R A 1964 *J. Chem. Phys.* **40** 1686
[26] O'Connell J K and Lane N F 1983 *Phys. Rev.* A **27** 1893
[27] Padial N T and Norcross D W 1984 *Phys. Rev.* A **29** 1742
[28] Jain A and Baluja K L 1992 *Phys. Rev.* A **45** 202
[29] Kaur G, Jain A K, Mohan H, Singh P S, Sharma S and Tripathi A N 2015 *Phys. Rev.* A **91** 022702
[30] Gianturco F A, Rodriguez-Ruiz J A and Sanna N 1995 *Phys. Rev.* A **52** 1257
[31] Cowan R 1981 *The Theory of Atomic Structure and Spectra* (Berkeley, CA: University of California Press) p 731
[32] Sin Fai Lam L T 1982 *J. Phys. B: At. Mol. Phys.* **15** 119
[33] Radzig A A and Smirnov B M 1985 *Reference Data on Atoms, Molecules, and Ions* (Berlin: Springer) p 466
[34] Staszewska G, Schwenke D W and Truhlar D G 1984 *Phys. Rev.* A **29** 3078
[35] Schwerdtfeger P 2016 Table of experimental and calculated static dipole polarizabilities for the electronic ground states of the neutral elements (in atomic units) (http://ctcp.massey.ac.nz/dipole-polarizabilities)
[36] Frisch M J *et al* 2009 *Gaussian 09, Revision E.01* (Wallingford, CT: Gaussian)
[37] Baran E J 2008 *J. Fluor. Chem.* **129** 1060–72
[38] Verma P and Antony B 2016 *J. Electr. Spectr. and Rel. Phenom.* **210** 30–5
[39] *NIST Computational Chemistry Comparison and Benchmark Database, NIST Standard Reference Database Number 101 Release 17b* 2015 ed Russell D Johnson III (http://cccbdb.nist.gov/polcalc2.asp)
[40] Schmidt M W *et al* 1993 *J. Comput. Chem.* **14** 1347
[41] Bode B M and Gordon M S 1998 *J. Mol. Graphics Mod.* **16** 133–8
[42] Christophorou L G and Olthoff J K 2004 *Fundamental Electron Interactions with the Plasma Processing Gases* (New York: Kluwer) p 776